A method to estimate the pre-eruptive water content of basalts:

application to the Wudalianchi–Erkeshan–Keluo volcanic field,

Northeastern China

(Supplemental Materials)

Yankun Di[1,a] , Wei Tian[1,*], Mimi Chen[1], Zefeng Li[2,b], Zhuyin Chu[3], Ju Liang[1]

[1]School of Earth and Space Sciences, Peking University, Beijing 100871, China

[2]School of Physics, Peking University, Beijing 100871, China

[3]State Key Laboratory of Lithospheric Evolution, Institute of Geology and Geophysics, Chinese Academy of Sciences, Beijing 100029, China

[a]Present address: Research School of Earth Sciences, Australian National University, Acton ACT 2601, Australia

[b]Present address: Research School of Astronomy & Astrophysics, Australian National University, Weston Creek, ACT 2611, Australia

[*]Corresponding author, email: davidtian@pku.edu.cn

Contents:

Appendix A. Analytical methods and results

Appendix B. Discussions on clinopyroxene–melt equilibrium

Appendix C. Discussions on water content estimation method

References cited

Table S1. Elemental compositions of the WEK basalts.

Table S2. Rb–Sr, Sm–Nd isotopic compositions of the WEK basalts.

Table S3. Clinopyroxene compositions of the WEK basalts.

Figure S1.

Figure S2.

Figure S3.

Figure S4.

Figure S5.

Appendix A. Analytical methods and results

The rock samples were initially sawn to remove altered and contaminated surfaces. Then the fresh rock blocks were sawn into thin chips. All the thin chips were visually checked to make sure they contained no impurities such as amygdales and xenocrysts. The samples were then sealed in several plastic bags and crushed into small chips using a hammer that was also wrapped in plastic bags. The plastic bags sealing the chips were replaced by new ones as soon as one layer of plastic had broken. After the chips had been hammered to fragments less than 5 mm in size, they were checked for small impurities again. Any chips with impurities were removed to guarantee purity. Then the purified chips were cleaned with 10% hydrochloric acid in an ultrasonic bath for approximately half an hour. After ultrasonification, the chips were cleaned three times with deionized water. Subsequently, selected rock chips were crushed using an alumina ceramic jaw crusher, then ground into fine powder with agate shatter-boxes. Finally, 20–30 g of powder was produced for each sample.

Elemental analyses

Major-element data for whole rock samples were obtained by X-ray fluorescence spectrometry on fused glass disks using an Axios-Minerals instrument at the Institute of Geology and Geophysics, Chinese Academy of Sciences (IGGCAS), following the procedures of Chu et al. (2009). Precision was 1%–3% RSD for elements present at >1 wt%, and approximately 10% RSD for elements present at <1 wt%. A Chinese basalt reference material, GSR-3, was analyzed during the same period, and the values determined were well within the range of consensus values (GeoREM, http://georem.mpch-mainz.gwdg.de/; Table S1).

Trace-element concentrations, including rare earth elements (REE), were determined by

inductively coupled plasma mass spectrometry using an Agilent 7500a system at IGGCAS, following the procedures described in Chu et al. (2009). Basalt reference materials BHVO-2 and BCR-2 were measured to monitor the accuracy of the analytical procedure; the results were in good agreement with reference values (GeoREM, http://georem.mpch-mainz.gwdg.de/; Table S1). Precision was generally better than 3% for most elements based on replicate analyzes of several samples.

Sulfur concentrations were determined at the National Research Center for Geoanalysis, Chinese Academy of Geological Sciences, using a high-frequency infrared absorption spectrometer (HIR-944B, Wuxi High-speed Analyzer Co. Ltd., China), following the procedures described in Chu et al. (2009). The detection limit for S was approximately 50 ppm.

Sr–Nd isotope analyses

Sr and Nd isotope compositions were determined at the State Key Laboratory of Lithospheric Evolution, Institute of Geology and Geophysics, Chinese Academy of Sciences. A combined chemical procedure for Rb–Sr and Sm–Nd isotopic analyzes from one-sample digestion was used, as described in detail by Yang et al. (2010). The Rb–Sr and Sm–Nd isotopic analyzes were conducted using an Isoprobe-T thermal ionization mass spectrometer made by Isotopx Company (formerly GV instruments). Measured $^{87}Sr/^{86}Sr$ and $^{143}Nd/^{144}Nd$ ratios were corrected for mass-fractionation using $^{86}Sr/^{88}Sr = 0.1194$ and $^{146}Nd/^{144}Nd = 0.7219$. During the period of data collection, the measured values for the NBS-987 Sr standard and the JNdi-1 Nd standard were $^{87}Sr/^{86}Sr = 0.710245 \pm 16$ (2 SD, n = 8) and $^{143}Nd/^{144}Nd = 0.512117 \pm 10$ (2 SD, n = 8). The USGS basalt reference materials BCR-2 and BHVO-2 were measured for Rb–Sr and Sm–Nd isotopic compositions to monitor the accuracy of the analytical procedures; the results were in excellent

agreement with the reported reference values (GeoREM, http://georem.mpch-mainz.gwdg.de/; Table S2). The procedural blanks were approximately 40 pg for Rb, 300 pg for Sr, 20 pg for Sm, and 60 pg for Nd.

Mineral chemistry analyses

Major-element compositions of clinopyroxenes were analyzed with a JXA-8100 electron microprobe at Peking University in wavelength dispersive mode with 15 kV acceleration potential, 10 nA beam current, and a beam diameter of 1 micrometer. Matrix corrections were carried out using the PRZ correction program. Back-scattered electron (BSE) images were taken simultaneously with the JXA-8100.

Results

The major- and trace-element contents of the samples are presented in Table S1. Consistent with previous reports (Zhang et al. 1995; Zou et al. 2003; Chen et al. 2007; Chu et al. 2013; Sun et al. 2014), these potassic rocks have relatively low Al_2O_3 and CaO contents for a given MgO content compared to other Cenozoic basalts in NE China (Fig. S2). The WEK basalts have REE and large ion lithophile element (LILE) concentrations higher than other Cenozoic basalts in NE China and ocean island basalts. On a chondrite-normalized REE diagram (Fig. S3a), the WEK basalts show uniform REE characteristics with strong light REE enrichment [$(La/Yb)_N = 42.5$–57.2] relative to CI chondrite [$(La/Yb)_N = 1$] and ocean island basalts (OIB) [$(La/Yb)_N = 12.3$, Sun and McDonough 1989]. The heavy REEs are also strongly fractionated with $(Sm/Yb)_N = 9.1$–11.8 [cf. OIB $(Sm/Yb)_N = 5.1$, Sun and McDonough 1989]. These samples have uniform primitive-mantle-normalized trace-element patterns (Fig. S3b), with strong enrichment of LILE

(sample/primitive mantle > 100) and Pb and K (sample/primitive mantle > 200), slight enrichment of Zr and Hf (sample/primitive mantle ≈ 50), and significant depletion of U, Th, Nb, and Ta compared to adjacent elements in the diagram.

The Sr and Nd isotopic compositions of the WEK basalts are listed in Table S2. The Sr–Nd isotopes of the WEK basalts are more enriched (i.e., Sr isotopic compositions are more radiogenic and Nd isotopic compositions are less radiogenic) than Cenozoic basalts elsewhere in NE China (Fig. S4). Consistent with previously reported results (Zhang et al. 1995; Zou et al. 2003), $^{87}Sr/^{86}Sr$ is negatively correlated with $^{143}Nd/^{144}Nd$, overlapping the enriched mantle 1 (EM1) oceanic basalt field (Zindler and Hart 1986; Fig. S4).

The clinopyroxene mineral compositions and pressure–temperature (P–T) calculation results based on the clinopyroxene–melt thermobarometer are listed in Table S3.

Appendix B. Discussions on clinopyroxene–melt equilibrium

Equilibrium tests

In a magma process, the "equilibrium" between clinopyroxene and the melt includes three cases: 1) a clinopyroxene grain crystallized from a melt and its composition did not change after crystallization; 2) after crystallization, the clinopyroxene grain reacted with, dissolved in, and re-equilibrated with the melt; 3) a clinopyroxene grain from other magma or the wall rock reacted with the melt and reached equilibrium during mixing or assimilation processes. In the first case, if the clinopyroxene is the liquidus mineral, its composition can be matched with that of the whole rock, whereas in the second and third cases the reactions modify the equilibrium melt compositions. In these latter cases, the equilibrium melt may be the matrix/glass (e.g., Jankovics et al. 2015; Winpenny and McLennan 2011), or the whole rock composition with subtraction of some early

crystallized minerals. Several approaches to test whether a melt is appropriate to pair with a clinopyroxene grain are discussed below.

The most essential test is to check the mineral–liquid Fe–Mg exchange equilibrium (e.g., K_D(Fe–Mg)$^{cpx–liq}$ = 0.28; Putirka 2008). If the whole rock is not in equilibrium with a clinopyroxene, early crystallized minerals may be subtracted until equilibrium is obtained (e.g., Putirka 1997; Armienti et al. 2013; Tao et al. 2015). An alternative method is to select liquid compositions from the whole rock and glass-composition database of the study area (e.g., Winpenny and McLennan 2011; Neave et al. 2013). However, Fe–Mg exchange equilibrium only indicates that the liquid is likely to be equilibrated with the clinopyroxene, but does not guarantee this equilibrium. An arbitrarily selected liquid, or a liquid with some olivine subtracted, may be adjusted to Fe–Mg exchange equilibrium with a given clinopyroxene, but may not be in equilibrium with other elements, such as Al, Ca, and Na (Putirka 2008). In addition, Putirka et al. (2009) and Mollo et al. (2013) demonstrated that under rapid crystallization conditions disequilibrium of clinopyroxene composition was observed. This disequilibrium originated from chemical kinetic factors, but not modification of liquid composition. In both cases, the liquid compositions generated by subtracting olivine from "seemingly disequilibrated liquids" are not real, and thus the P–T estimates based on them are meaningless. Also, as shown by Putirka (1999, 2008), Putirka et al. (2003), Toplis (2005), and Herzberg and Asimow (2008), the Fe–Mg exchange constant of mineral with melt is a function of the pressure, temperature, and composition of both mineral and melt.

Another clinopyroxene–liquid equilibrium test is to predict the equilibrated clinopyroxene composition using models (e.g., Ghiorso et al. 2002; Putirka 1999; Mollo et al. 2013) with the candidate liquid composition and the calculated pressure and temperature. If the predicted

clinopyroxene composition is consistent with the measured compositions, equilibrium is thought to be reached. If not, some early crystallized minerals must be subtracted until the consistency is reached. The effectiveness of this method was demonstrated by Putirka and Condit (2003), Putirka et al. (2009), Stroncik et al. (2009), Hildner et al. (2011), Dahren et al. (2012), and Barker et al. (2015). Theoretically this approach guarantees mineral–melt equilibrium, but as the thermobarometer models and the prediction models use different calibrating datasets, systematic errors may exist between models.

A very different perspective to test equilibrium is to predict the clinopyroxene saturation temperatures with the liquid composition by means of models (e.g., Ghiorso et al. 2002; Putirka 1999; Mollo et al. 2013) and to compare them with the calculated temperatures, as applied by Putirka and Condit (2003), Putirka et al. (2009), and Armienti et al. (2013). If a clinopyroxene grain did not undergo re-equilibrating processes with the melt after crystallization, the calculated temperature and pressure obtained using thermobarometers should be on the clinopyroxene saturation surface of the liquid used for the $P–T$ calculation. However, the position of the clinopyroxene saturation surface of a given melt composition is sensitive to the H_2O content. Therefore, if the calculated temperature from the thermobarometer is under the predicted saturation surface, this liquid is not the equilibrium melt, and two alternative conclusions may be drawn: reaction of mineral and melt occurred; or volatiles, such as H_2O, were present. Subtraction of olivine from a volatile-bearing liquid to fit the calculated temperature to the saturation surface may also lead to incorrect $P–T$ estimates. In addition, volatile-bearing magmas are usually related to explosion and rapid ascent in the lithosphere, leading to fast crystallization and kinetics-originated disequilibrium.

The fourth equilibrium-checking method is to apply another thermobarometer, such as the

olivine–liquid thermometer (Beattie 1993; Putirka 1997; Putirka et al. 2007) or the Si activity thermobarometer (Putirka 2008; Lee et al. 2009), to obtain an independent P–T estimate. If the results of different thermobarometers overlap with each other, the P–T estimates are highly likely to be robust. This equilibrium test was utilized by Putirka (1997), Putirka and Condit (2003), Stroncik et al. (2009), Putirka et al. (2009), and Tao et al. (2015).

In summary, to use the clinopyroxene–melt thermobarometer correctly, the clinopyroxene and melt pairs must be in equilibrium. Methods of checking clinopyroxene–melt equilibrium include: 1) checking the Fe–Mg exchange equilibrium constant; 2) predicting the equilibrated clinopyroxene composition with the liquid used for P–T calculation as well as the calculated P–T result; 3) predicting the saturation surface of the liquid; and 4) using another independent thermobarometer.

Effects of clinopyroxene zoning

Compositional zoning is a common phenomenon in igneous crystals. Complex zoning patterns in clinopyroxene phenocrysts may reflect elongated crystallization history and/or open system behavior, thus can cause problems in the application of clinopyroxene–melt thermobarometer. For a zoned clinopyroxene crystal, which composition zone should be used for P–T calculation is an important question needs to be answered.

The formation of zoning texture in igneous crystals generally includes four cases: (1) melt composition change due to crystallization following a liquid line of descent (normal zoning); (2) resorption, re-equilibration, and recrystallization of existing crystal due to changes of P, T, f_{O2}, or volatile content (core-rim or core-mantle structure); (3) kinetic-controlled small-scale composition oscillation during crystal growth (sector and oscillatory zoning); (4) melt composition change due

to magma mixing and assimilation (reverse zoning, patchy zoning, growth bands, etc.). In these cases, (1)–(3) can occur in closed system magma evolutions, whereas (4) requires an open system.

For clinopyroxene zoning in case (1), the inner zones are expected to equilibrate a more primary melt (e.g., bulk rock), whereas the outer zones are expected to equilibrate a more evolved melt (e.g., glass in contact with the rim of crystal). Thus, different melts should be selected for these zones in P–T calculation. If the crystallinity of the magma is sufficiently low and the change of melt composition due to crystallization is negligible, both inner and outer zones can be paired with the observed melt in P–T calculation. The same argument applies to case (2). In case (3), the sector and oscillatory zoning of clinopyroxene reflects the variations of small-scale kinetic effects during crystal growth, such as solute diffusion rate, extent of oversaturation, interface effect, and lattice stress, rather than large-range melt composition/condition changes (Downes 1974; Shore and Fowler 1996). Disequilibrium partitioning of Fe, Mg, Al, Ca, Na may result from these kinetic effects (Putirka et al. 2009; Mollo et al. 2013; Neave and Putirka 2017). Nonetheless, these different zones all grow from the same melt at the same condition, thus they should record the same P–T (if they equilibrate the melt). Therefore, in cases (1)–(3), all zones of a clinopyroxene phenocryst can be used for P–T calculation, *as long as they are checked to be in equilibrium with the right melt composition*. Zoning in case (4), however, is a problem for thermobarometry, because the melt composition is altered in open system (magma mixing/assimilation), and the endmembers and extents of magma mixing/assimilation are unknown. Using the observed melt composition for the thermobarometer will result in problematic P–T results.

For the WEK samples studied here, actually most clinopyroxene phenocrysts are small (all phenocrysts < 0.5 mm, most phenocrysts < 0.1 mm) and unzoned. Only seven large euhedral, large, zoned phenocrysts are found in our carefully checked ~10 rock thin sections, with the one shown

in Fig. 2a the most representative. For these phenocrysts, we performed multi-spot analyses, followed by selection of equilibrated zones using the equilibrium filters. We consider each zone as an individual clinopyroxene crystallized from the common melt, because the zoning found in our samples most likely belongs to the aforementioned cases (1)–(3) rather, than case (4), based on three observations. Firstly, the clinopyroxene zoning pattern, as represented by Fig. 2a, is similar to the description of oscillatory zoning (Shore and Fowler 1996; Streck 2008): multiple growth layers parallel to crystallographic planes of low Miller indices, concentric with the external margin of crystal, and layer thickness of 1–10 μm. The zoning texture is only recognizable in back-scattered electron images by forcing the contrast very high, probably because the overall atomic mass change in ion substitutions is small. Secondly, different zones from the same crystals yielded identical P–T estimates within error. Take the phenocryst in Fig. 2a as an example, three spots analyzed at outer, intermediate, and inner zones yielded pressures of 3.3±1.7, 5.1±1.7, and 3.5±1.7 kbar respectively. Thirdly, abundant evidence has rule out magma mixing and crustal assimilation for the WEK magmas, such as the near-primitive melt composition, high magma ascent rate suggested by the common occurrence of mantle xenoliths and significant [230]Th excess (Zou et al. 2003), and the uncontaminated mantle Os isotope signatures (Chu et al. 2013; Sun et al. 2014). We therefore conclude that the occurrence of zoning in our samples does not trouble the P–T calculation. All compositional zones can potentially be used for P–T calculation, as long as they pass the equilibrium test.

Appendix C. Discussions on water content estimation method

A flow chart of our water content estimation using the two thermobarometers is shown in Fig. S5. The estimation method is generally composed of three calculation steps: (a) P–T

calculation using the Putirka et al. (2003) clinopyroxene–melt thermobarometer; (b) P–T calculation using the Lee et al. (2009) Si activity thermobarometer with an assumed H_2O content; and (c) Evaluating the consistency of the two sets of P–T estimates. The calculation steps are consecutively repeated, with the H_2O content used in (b) varying within a given range by a set increment. The H_2O content that maximizes the consistency in (c) will be the best estimation value.

Data filtering and correction are needed before implementing the H_2O content estimation. Step (a) requires input of equilibrated clinopyroxene–melt pairs. The selection of potential melt compositions and equilibrated pairs have been discussed in Appendix B. Step (b) requires melt compositions in equilibrium with olivine and orthopyroxene (ol+opx) as input. This ol+opx assemblage is from the mantle in most cases, but it can also be the fractionated crystals from the melt or solidified predecessor melts in the magma conduit. The melt–mantle equilibrium can be tested by Fe–Mg exchange between the silicate melt and mantle olivine. Magma f_{O2} (or melt Fe^{3+}/Fe^{Total}), mantle Fo, and $K_D(Fe–Mg)^{ol–melt}$ values are required for the equilibrium test and reverse crystallization correction if the melt experienced olivine-only-controlled fractionation. The models involved in the test and the correction approaches are recently discussed by Putirka (2016) and Plank and Forsyth (2016).

The core of the H_2O content estimation method is step (c). The consistency of the two sets of P–T estimates can be evaluated by several proxies. The simplest one is the absolute temperature difference, $|\Delta T|$, derived from direct comparison of T estimates with same P, as shown in Table 1. A second proxy is the distance of the two regressed P–T trends in slope–intercept space, if the P–T arrays given by both thermobarometers show good linearity. Alternatively, the two sets of P–T arrays can be regressed together, and the global goodness-of-fit (MSWD or R^2) can be used as a quantitative indicator. However, the two thermobarometers do not always give perfectly matched

pressure results or linear *P–T* trends, thus these proxies are not applicable at all times. We alternatively look at the overlapping degree of the two *P–T* arrays with consideration of their errors, and express it by buffer overlapping area (BOA). Once the buffers for the two thermobarometers are constructed by outlining error ellipses (Fig. 4a), their overlapping area in *P–T* space can be calculated or measured. Analytically solving the overlapping area of two ellipses is difficult, not to mention an ensemble of a series of ellipses. Therefore, a numerical discretization mothod is employed in our method. The buffers are separated into tiny rectangle units (i.e., 2-dimensional bins), and the BOA is approximated by unit counting. Obviously, a finer division of units will lead to a more precise numerical solution but inevitably longer program running time. In practice, we adopt a rectangle unit size with long side and short side lengths of ca. 10% of the semi major axis and semi minor axis lengths of the ellipses, respectively. The Python code of our water content estimation method with a user manual is available at https://github.com/zidianjun/BOA_calculation.

Restrictions apply to the application of this method. The volcanic rock samples suitable for H_2O content estimation with this method should be free from crustal contamination, and should not be far from the olivine-controlled liquid line of decent. Low crystallinity samples (e.g., phenocryst < 5%) with unzoned clinopyroxene phenocrysts are expected to perform well. The H_2O content estimation will fail if the two *P–T* arrays have no overlap (i.e., BOA = 0) in the entire assumed H_2O content range. This may happen if the depths of melt–ol–opx equilibria (e.g., deep mantle) are much greater than the depths of clinopyroxene crystallization (e.g., shallow crust or surface). In this case, other proxies or thermobarometers may be considered.

It should be noted that the water content estimation method reported in this study is by no means a replacement for more accurate methods of H_2O analysis (FTIR, SIMS, etc.), but it has the

advantage of applicability in cases where no primary melt inclusion exist. The principle of this method is the P–T–X–H_2O relation of mineral–melt equilibrium, similar to the geohygrometers recently developed by Armienti et al. (2013) and Gavrilenko et al. (2016). Such hygrometers can be expressed and calibrated as function $H_2O = f(X^{mineral}, X^{melt}, P, T)$ in general. The difficulty in practice is, however, to independently determine P and T of the equilibrium. In the clinopyroxene hygrometer of Armienti et al. (2013), P and T were derived from the Putirka et al. (2003) thermobarometry of the same clinopyroxene. However, melt compositions were not considered in this hygrometer; it was only empirically calibrated on Etnean melt compositions. This obstructs its application to other volcanos with different melt compositions and H_2O contents. In the Ca-in-olivine hygrometer of Gavrilenko et al. (2016), it was assumed that both P and T can be completely accounted for by the melt MgO content, which is just a first-order approximation. This hygrometer is potentially affected by issues such as Ca diffusion and secondary Ca fluorescence from glass, and further investigations are needed. Different from these two hygrometers, our method employs the melt Si activity equilibrium as an expression of H_2O, and use another completely independent (i.e., clinopyroxene–melt) equilibrium system to produce P and T estimates. The P and T estimates are not for specific Si activity equilibria, but correspond to the P–T path of magma ascending. The accuracy of H_2O content estimation by this method relies on the accuracy and consistency of the two thermobarometers. Better calibrations, or other better volcanic thermobarometers (e.g., feldspar–melt, orthopyroxene–melt, two-pyroxene), may replace the thermobarometers employed here to achieve better H_2O content estimation accuracy.

References cited

Armienti, P., Perinelli, C., and Putirka, K.D. (2013) A new model to estimate deep-level magma

ascent rates, with applications to Mt. Etna (Sicily, Italy). Journal of Petrology, 54(4), 795-813.

Barker, A.K., Troll, V.R., Carracedo, J.C., and Nicholls, P.A. (2015) The magma plumbing system for the 1971 Teneguia eruption on La Palma, Canary Islands. Contributions to Mineralogy and Petrology, 170(5-6).

Basu, A.R., Wang, J.W., Huang, W.K., Xie, G.H., and Tatsumoto, M. (1991) Major element, REE, and Pb, Nd and Sr isotopic geochemistry of cenozoic volcanic-rocks of eastern China - implications for their origin from suboceanic-type mantle reservoirs. Earth and Planetary Science Letters, 105(1-3), 149-169.

Beattie, P. (1993) Olivine-melt and orthopyroxene-melt equilibria. Contributions to Mineralogy and Petrology, 115(1), 103-111.

Chen, Y., Zhang, Y.X., Graham, D., Su, S.G., and Deng, J.F. (2007) Geochemistry of Cenozoic basalts and mantle xenoliths in Northeast China. Lithos, 96(1-2), 108-126.

Chen, H., Xia, Q.-K., Ingrin, J., Jia, Z.-B., and Feng, M. (2015) Changing recycled oceanic components in the mantle source of the Shuangliao Cenozoic basalts, NE China: New constraints from water content. Tectonophysics, 650, 113-123.

Chu, Z.Y., Wu, F.Y., Walker, R.J., Rudnick, R.L., Pitcher, L., Puchtel, I.S., Yang, Y.H., and Wilde, S.A. (2009) Temporal evolution of the lithospheric mantle beneath the eastern North China Craton. Journal of Petrology, 50(10), 1857-1898.

Chu, Z.Y., Harvey, J., Liu, C.Z., Guo, J.H., Wu, F.Y., Tian, W., Zhang, Y.L., and Yang, Y.H. (2013) Source of highly potassic basalts in northeast China: Evidence from Re-Os, Sr-Nd-Hf isotopes and PGE geochemistry. Chemical Geology, 357, 52-66.

Dahren, B., Troll, V.R., Andersson, U.B., Chadwick, J.P., Gardner, M.F., Jaxybulatov, K., and

Koulakov, I. (2012) Magma plumbing beneath Anak Krakatau volcano, Indonesia: evidence for multiple magma storage regions. Contributions to Mineralogy and Petrology, 163(4), 631-651.

Downes, M.J. (1974) Sector and oscillatory zoning in calcic augites from Mt-Etna, Sicily. Contributions to Mineralogy and Petrology, 47(3), 187-196.

Gavrilenko, M., Herzberg, C., Vidito, C., Carr, M.J., Tenner, T., and Ozerov, A. (2016) A calcium-in-olivine geohygrometer and its application to subduction zone magmatism. Journal of Petrology, 57(9), 1811-1831.

Ghiorso, M.S., Hirschmann, M.M., Reiners, P.W., and Kress, V.C. (2002) The pMELTS: A revision of MELTS for improved calculation of phase relations and major element partitioning related to partial melting of the mantle to 3 GPa. Geochemistry Geophysics Geosystems, 3.

Herzberg, C., and Asimow, P.D. (2008) Petrology of some oceanic island basalts: PRIMELT2.XLS software for primary magma calculation. Geochemistry Geophysics Geosystems, 9.

Hildner, E., Kluegel, A., and Hauff, F. (2011) Magma storage and ascent during the 1995 eruption of Fogo, Cape Verde Archipelago. Contributions to Mineralogy and Petrology, 162(4), 751-772.

Jankovics, M.E., Harangi, S., Nemeth, K., Kiss, B., and Ntaflos, T. (2015) A complex magmatic system beneath the Kissomlyo monogenetic volcano (western Pannonian Basin): evidence from mineral textures, zoning and chemistry. Journal of Volcanology and Geothermal Research, 301, 38-55.

Le Bas, M.J., Le Maitre, R.W., Streckeisen, A., and Zanettin, B. (1986) A chemical classification of volcanic-rocks based on the total alkali silica diagram. Journal of Petrology, 27(3), 745-

750.

Lee, C.T.A., Luffi, P., Plank, T., Dalton, H., and Leeman, W.P. (2009) Constraints on the depths and temperatures of basaltic magma generation on Earth and other terrestrial planets using new thermobarometers for mafic magmas. Earth and Planetary Science Letters, 279(1-2), 20-33.

Liu, C.Q., Masuda, A., and Xie, G.H. (1994) Major-element and trace-element compositions of cenozoic basalts in Eastern China - petrogenesis and mantle source. Chemical Geology, 114(1-2), 19-42.

Liu, J.Q., Han, J.T., and Fyfe, W.S. (2001) Cenozoic episodic volcanism and continental rifting in northeast China and possible link to Japan Sea development as revealed from K-Ar geochronology. Tectonophysics, 339(3-4), 385-401.

Mollo, S., Putirka, K., Misiti, V., Soligo, M., and Scarlato, P. (2013) A new test for equilibrium based on clinopyroxene-melt pairs: Clues on the solidification temperatures of Etnean alkaline melts at post-eruptive conditions. Chemical Geology, 352, 92-100.

Neave, D.A., and Putirka, K.D. (2017) A new clinopyroxene-liquid barometer, and implications for magma storage pressures under Icelandic rift zones. American Mineralogist, 102(4), 777-794.

Neave, D.A., Passmore, E., Maclennan, J., Fitton, G., and Thordarson, T. (2013) Crystal-melt relationships and the record of deep mixing and crystallization in the ad 1783 Laki eruption, Iceland. Journal of Petrology, 54(8), 1661-1690.

Plank, T., and Forsyth, D.W. (2016) Thermal structure and melting conditions in the mantle beneath the Basin and Range province from seismology and petrology. Geochemistry Geophysics Geosystems, 17(4), 1312-1338.

Putirka, K. (1997) Magma transport at Hawaii: Inferences based on igneous thermobarometry. Geology, 25(1), 69-72.

——. (1999) Clinopyroxene plus liquid equilibria to 100 kbar and 2450 K. Contributions to Mineralogy and Petrology, 135(2-3), 151-163.

——. (2008) Thermometers and barometers for volcanic systems. In K.D. Putirka, and F.J. Tepley, Eds. Minerals, Inclusions and Volcanic Processes, 69, p. 61-120. Mineralogical Soc Amer, Chantilly.

——. (2016) Rates and styles of planetary cooling on Earth, Moon, Mars, and Vesta, using new models for oxygen fugacity, ferric-ferrous ratios, olivine-liquid Fe-Mg exchange, and mantle potential temperature. American Mineralogist, 101(3-4), 819-840.

Putirka, K., and Condit, C.D. (2003) Cross section of a magma conduit system at the margin of the Colorado Plateau. Geology, 31(8), 701-704.

Putirka, K.D., Mikaelian, H., Ryerson, F., and Shaw, H. (2003) New clinopyroxene-liquid thermobarometers for mafic, evolved, and volatile-bearing lava compositions, with applications to lavas from Tibet and the Snake River Plain, Idaho. American Mineralogist, 88(10), 1542-1554.

Putirka, K.D., Perfit, M., Ryerson, F.J., and Jackson, M.G. (2007) Ambient and excess mantle temperatures, olivine thermometry, and active vs. passive upwelling. Chemical Geology, 241(3-4), 177-206.

Putirka, K.D., Kuntz, M.A., Unruh, D.M., and Vaid, N. (2009) Magma evolution and ascent at the craters of the Moon and neighboring volcanic fields, southern Idaho, USA: Implications for the evolution of polygenetic and monogenetic volcanic fields. Journal of Petrology, 50(9), 1639-1665.

Sakuyama, T., Tian, W., Kimura, J.I., Fukao, Y., Hirahara, Y., Takahashi, T., Senda, R., Chang, Q., Miyazaki, T., Obayashi, M., and others. (2013) Melting of dehydrated oceanic crust from the stagnant slab and of the hydrated mantle transition zone: Constraints from Cenozoic alkaline basalts in eastern China. Chemical Geology, 359, 32-48.

Streck, M.J. (2008) Mineral textures and zoning as evidence for open system processes. In K.D. Putirka, and F.J. Tepley, Eds. Minerals, Inclusions and Volcanic Processes, 69, p. 595-622.

Stroncik, N.A., Kluegel, A., and Hansteen, T.H. (2009) The magmatic plumbing system beneath El Hierro (Canary Islands): constraints from phenocrysts and naturally quenched basaltic glasses in submarine rocks. Contributions to Mineralogy and Petrology, 157(5), 593-607.

Sun, S.S., and McDonough, W.F. (1989) Chemical and isotopic systematics of oceanic basalts: implications for mantle composition and processes. Geological Society London Special Publications, 42(1), 313-345.

Sun, Y., Ying, J.F., Zhou, X.H., Shao, J., Chu, Z.Y., and Su, B.X. (2014) Geochemistry of ultrapotassic volcanic rocks in Xiaogulihe NE China: Implications for the role of ancient subducted sediments. Lithos, 208, 53-66.

Tang, Y.J., Zhang, H.F., and Ying, J.F. (2006) Asthenosphere-lithospheric mantle interaction in an extensional regime: Implication from the geochemistry of Cenozoic basalts from Taihang Mountains, North China Craton. Chemical Geology, 233(3-4), 309-327.

Tao, Y., Putirka, K., Hu, R.Z., and Li, C.S. (2015) The magma plumbing system of the Emeishan large igneous province and its role in basaltic magma differentiation in a continental setting. American Mineralogist, 100(11-12), 2509-2517.

Toplis, M.J. (2005) The thermodynamics of iron and magnesium partitioning between olivine and liquid: criteria for assessing and predicting equilibrium in natural and experimental systems.

Contributions to Mineralogy and Petrology, 149(1), 22-39.

Winpenny, B., and MacLennan, J. (2011) A partial record of mixing of mantle melts preserved in Icelandic phenocrysts. Journal of Petrology, 52(9), 1791-1812.

Xu, Y.G., Ma, J.L., Frey, F.A., Feigenson, M.D., and Liu, J.F. (2005) Role of lithosphere-asthenosphere interaction in the genesis of Quaternary alkali and tholeiitic basalts from Datong, western North China Craton. Chemical Geology, 224(4), 247-271.

Xu, Z., Zhao, Z.F., and Zheng, Y.F. (2012) Slab-mantle interaction for thinning of cratonic lithospheric mantle in North China: Geochemical evidence from Cenozoic continental basalts in central Shandong. Lithos, 146, 202-217.

Yan, J., and Zhao, J.X. (2008) Cenozoic alkali basalts from Jingpohu, NE China: The role of lithosphere-asthenosphere interaction. Journal of Asian Earth Sciences, 33(1-2), 106-121.

Yang, Y.H., Zhang, H.F., Chu, Z.Y., Xie, L.W., and Wu, F.Y. (2010) Combined chemical separation of Lu, Hf, Rb, Sr, Sm and Nd from a single rock digest and precise and accurate isotope determinations of Lu-Hf, Rb-Sr and Sm-Nd isotope systems using Multi-Collector ICP-MS and TIMS. International Journal of Mass Spectrometry, 290(2-3), 120-126.

Zhang, J.B. (1992) Source's characteristics of ultra-potassium basaltic rocks from northeast China and research on regional mantle geochemistry. Ph.D. thesis, Institute of Geology, Chinese Academy of Sciences, Beijing (in Chinese).

Zhang, M., Suddaby, P., Thompson, R.N., Thirlwall, M.F., and Menzies, M.A. (1995) Potassic volcanic-rocks in NE China - geochemical constraints on mantle source and magma genesis. Journal of Petrology, 36(5), 1275-1303.

Zhao, Y.W., Li, N., Fan, Q.C., Zou, H.B., and Xu, Y.G. (2014) Two episodes of volcanism in the Wudalianchi volcanic belt, NE China: Evidence for tectonic controls on volcanic activities.

Journal of Volcanology and Geothermal Research, 285, 170-179.

Zindler, A., and Hart, S. (1986) Chemical geodynamics. Annual Review of Earth and Planetary Sciences, 14, 493-571.

Zou, H.B., Reid, M.R., Liu, Y.S., Yao, Y.P., Xu, X.S., and Fan, Q.C. (2003) Constraints on the origin of historic potassic basalts from northeast China by U-Th disequilibrium data. Chemical Geology, 200(1-2), 189-201.

Table S1 Elemental compositions of the WEK basalts.

Sample	SC1	SC2	GST1	GST2	GST3	GST5	KL1	KL2
Age	1719–1721 A.D.		0.42 Ma (Zhao et al. 2014)				0.13 Ma (Liu et al. 2001)	
Location	48°42'13.33" N		48°39'44.280" N				49°18'0.36" N	
	126°11'35.57" E		126°16'04.462" E				125°53'56.31" E	
Data source			This study					
Major elements (wt%)								
SiO_2	53.62	53.32	53.32	52.99	53.09	53.16	53.18	53.49
TiO_2	2.31	2.34	2.37	2.29	2.28	2.31	2.35	2.30
Al_2O_3	13.98	13.97	13.94	13.83	13.84	13.86	13.81	13.93
$TFe_2O_3{}^b$	8.14	8.21	8.61	8.57	8.63	8.63	8.22	8.13
MnO	0.10	0.11	0.10	0.10	0.11	0.11	0.11	0.11
MgO	5.94	5.97	6.46	6.71	6.76	6.74	5.99	5.97
CaO	5.05	5.10	5.45	5.62	5.61	5.63	5.12	5.04
Na_2O	3.95	3.94	3.76	3.65	3.70	3.73	3.98	3.94
K_2O	5.49	5.55	4.94	4.73	4.72	4.75	5.55	5.46
P_2O_5	0.97	0.97	0.93	0.88	0.85	0.87	0.98	0.96
LOI	–0.16	–0.06	0.18	0.22	0.22	0.10	0.84	0.04
TOTAL	99.39	99.42	100.1	99.59	99.80	99.88	100.1	99.37
K_2O/Na_2O	1.39	1.41	1.31	1.30	1.28	1.27	1.39	1.39
Mg#	66.7	66.7	67.4	68.3	68.3	68.2	66.7	66.9
Trace elements (ppm)								
Sc	12.6	12.6	10.5	11.0	11.1	11.0	12.8	10.2
Cr	175	177	210	224	233	227	375	64
Ni	150	149	156	167	169	167	288	60
Cu	34.4	34.3	29.7	32.7	33.4	34.7	22.1	27.2
Zn	112	112	113	109	110	110	112	119
Rb	111	110	92.4	89.4	89.6	91.5	99.6	122
Sr	1422	1406	1655	1570	1567	1584	1596	1532
Y	21.4	21.2	17.8	17.6	17.2	17.4	23.0	21.9
Zr	469	468	321	300	302	303	398	518
Nb	65.3	64.2	66.5	63.3	63.4	64.2	66.1	72.2
Ba	1715	1696	1747	1668	1665	1683	1866	1921
La	81.5	80.9	70.4	66.8	64.5	65.9	96.3	91.7
Ce	154	153	134	126	122	124	179	171
Pr	17.9	17.7	15.6	14.7	14.3	14.5	20.8	19.8
Nd	66.2	65.7	58.4	55.4	54.2	55.0	77.0	72.6
Sm	11.0	10.9	10.0	9.63	9.40	9.47	12.9	12.1

Eu	3.13	3.11	3.03	2.89	2.87	2.90	3.67	3.47
Gd	8.73	8.62	7.73	7.48	7.31	7.45	10.0	9.42
Tb	0.99	0.98	0.884	0.856	0.833	0.844	1.13	1.07
Dy	4.98	4.92	4.33	4.23	4.13	4.19	5.61	5.30
Ho	0.794	0.794	0.677	0.664	0.648	0.656	0.867	0.821
Er	1.91	1.89	1.55	1.55	1.52	1.55	2.01	1.91
Tm	0.226	0.226	0.179	0.178	0.178	0.176	0.229	0.219
Yb	1.29	1.25	1.01	0.979	0.981	0.969	1.21	1.19
Lu	0.168	0.166	0.128	0.131	0.131	0.128	0.155	0.152
Hf	10.4	10.4	6.90	6.44	6.44	6.49	8.9	11.6
Ta	3.67	3.72	3.80	3.65	3.67	3.76	3.73	4.25
Pb	14.7	14.6	11.3	10.7	10.7	10.6	13.9	17.6
Th	6.65	6.46	6.37	6.16	6.05	6.05	8.16	8.80
U	1.50	1.47	1.23	1.20	1.22	0.992	1.64	1.86
S	<50	<50	70	90	70	80	70	90

[a] Reported values for the reference materials are from GeoREM (http://georem.mpch-mainz.gwdg.de/).

[b] Total iron as Fe_2O_3; Mg# = $100 \times Mg^{2+}/(Mg^{2+} + Fe^{2+})$, assuming $Fe^{3+}/(Fe^{3+} + Fe^{2+})$ = 0.28.

(Continued)

YQ1	YQ3	YQ4	YQ6	YQ7	YQ8	LHS1	LHS3	LHS4	LHS6	HSS2	HSS5	HSS6	HSS8	KD1	KD3	KD4	KD5
Pleistocene (Zhang et al. 1995)							1719—1721 A.D.							0.56 Ma (Liu et al. 2001)			
48˚39.020' N			48˚39.326' N			48˚42.456' N			48˚43.061' N	48˚44.230' N		48˚44.665' N		48˚03.261' N			
126˚09.333' E			126˚08.973' E			126˚07.110' E			126˚07.645' E	126˚10.257' E		126˚11.056' E		126˚13.919' E			
									Chu et al. (2013)								
Major elements (wt%)																	
52.74	53.06	49.71	52.99	49.67	49.21	51.63	51.73	51.87	53.24	53.21	53.54	49.02	53.51	52.37	52.68	52.48	52.32
2.45	2.45	2.39	2.72	2.35	2.34	2.30	2.29	2.77	2.34	2.42	2.42	2.26	2.32	2.57	2.60	2.61	2.59
13.88	13.88	12.15	14.39	13.42	13.25	13.49	13.53	13.68	13.99	13.94	14.02	12.98	13.95	13.62	13.57	13.51	13.56
8.49	8.48	9.20	8.37	9.55	9.64	8.89	8.93	8.89	8.19	8.24	8.27	9.64	8.23	8.47	8.56	8.54	8.58
0.11	0.11	0.12	0.10	0.13	0.13	0.12	0.12	0.11	0.11	0.11	0.10	0.14	0.11	0.11	0.11	0.11	0.11
6.17	6.18	9.47	4.45	7.40	7.69	7.45	7.46	6.21	5.96	5.93	5.99	8.10	6.01	6.87	6.88	6.83	6.90
5.50	5.46	6.89	5.22	7.16	7.29	6.02	6.03	5.66	5.09	5.15	5.17	7.44	5.14	5.42	5.34	5.35	5.36
3.86	3.86	3.85	4.31	4.17	4.23	3.95	3.96	3.52	3.98	3.86	3.85	4.21	3.96	3.61	3.58	3.49	3.56
5.53	5.53	4.50	6.09	4.83	4.73	4.95	4.95	5.87	5.53	5.63	5.64	4.58	5.48	5.66	5.74	5.73	5.65
1.00	0.99	1.08	1.10	1.03	1.02	0.92	0.92	1.07	0.98	1.01	1.00	1.14	0.97	1.01	0.94	0.93	0.96
-0.04	-0.10	-0.02	-0.14	-0.14	-0.08	-0.18	-0.14	0.10	-0.02	-0.10	0.00	-0.16	-0.24	-0.04	-0.24	-0.14	-0.08

99.69	99.89	99.33	99.61	99.57	99.45	99.55	99.78	99.75	99.39	99.40	100.00	99.35	99.44	99.67	99.76	99.44	99.51
1.43	1.43	1.17	1.41	1.16	1.12	1.25	1.25	1.67	1.39	1.46	1.46	1.09	1.38	1.57	1.60	1.64	1.59
66.7	66.7	73.9	59.4	68.1	68.7	69.7	69.7	65.8	66.7	66.4	66.6	69.8	66.8	69.1	68.9	68.8	68.9

Trace elements (ppm)

11.7	12.3	12.1	12.2	12.2	11.7	12.2	12.1	13.8	14.4	14.5	14.1	12.9	13.4	13.2	13.0	13.1	13.1
190	194	193	187	185	186	182	181	171	265	195	218	241	242	210	214	211	209
158	161	161	159	157	155	156	156	134	207	151	164	185	185	161	162	161	163
31.8	33.3	32.1	32.5	32.3	31.9	33.2	33.0	30.4	38.1	35.2	32.3	35.1	36.6	41.0	38.2	36.0	39.1
114	118	116	116	115	109	116	114	112	122	119	120	111	111	105	108	108	107
107	111	110	111	110	110	114	112	116	92.3	100	96.6	101	101	111	109	110	108
1428	1486	1454	1470	1457	1456	1478	1447	1458	1752	1601	1641	1330	1336	1537	1583	1574	1571
21.8	22.5	22.1	22.2	22.1	22.0	22.1	21.7	22.2	26.7	24.2	24.4	21.1	21.3	21.0	19.8	19.7	20.0
524	533	530	533	529	529	521	511	518	391	389	382	415	418	491	496	495	491
66.6	69.0	68.0	68.1	68.1	68.0	67.3	66.0	68.9	72.0	70.6	71.5	64.3	64.3	65.6	66.6	66.7	66.6
1575	1628	1586	1616	1607	1613	1702	1675	1893	1835	1822	1842	1591	1596	1915	1941	1936	1941
84.5	87.5	85.7	86.3	85.8	86.4	85.9	84.5	84.0	104	91.6	93.1	75.5	76.1	84.8	78.8	78.2	80.0
160	166	162	163	163	162	163	161	160	193	171	174	143	144	160	148	148	152
18.5	19.1	18.7	18.8	18.7	18.7	18.9	18.4	18.5	22.3	19.8	20.1	16.5	16.7	18.4	17.2	17.2	17.6
67.7	70.0	68.6	69.3	69.2	69.3	69.8	68.6	68.0	83.2	74.0	75.1	61.7	62.7	67.6	63.2	63.3	64.5
11.2	11.6	11.3	11.5	11.5	11.4	11.6	11.4	11.2	13.9	12.5	12.8	10.6	10.7	11.1	10.2	10.3	10.5
3.18	3.28	3.21	3.23	3.21	3.22	3.27	3.21	3.19	3.98	3.66	3.71	3.05	3.08	3.21	3.10	3.11	3.12
8.87	9.14	8.86	8.93	8.92	8.91	9.05	8.77	8.82	11.1	10.0	10.3	8.43	8.56	8.64	8.11	8.14	8.27
1.01	1.03	1.01	1.02	1.03	1.02	1.03	1.00	0.99	1.25	1.15	1.17	0.98	0.99	0.97	0.906	0.911	0.93
5.14	5.28	5.22	5.24	5.17	5.19	5.22	5.06	5.08	6.35	5.74	5.88	4.96	4.98	4.85	4.57	4.58	4.65
0.818	0.843	0.831	0.828	0.831	0.829	0.829	0.815	0.817	1.001	0.913	0.926	0.801	0.812	0.783	0.741	0.746	0.759
1.97	2.03	1.99	1.97	1.97	1.96	1.98	1.92	1.95	2.33	2.12	2.14	1.89	1.90	1.89	1.77	1.77	1.82
0.232	0.244	0.236	0.237	0.236	0.240	0.236	0.228	0.231	0.269	0.248	0.250	0.225	0.224	0.227	0.213	0.217	0.217
1.31	1.34	1.31	1.31	1.32	1.33	1.29	1.29	1.30	1.46	1.34	1.34	1.24	1.28	1.29	1.22	1.25	1.26
0.174	0.180	0.174	0.175	0.171	0.179	0.173	0.171	0.176	0.198	0.180	0.179	0.170	0.172	0.176	0.164	0.169	0.170
11.6	11.8	11.7	11.8	11.6	11.7	11.6	11.3	11.4	8.5	8.5	8.40	9.2	9.4	10.8	10.7	10.9	10.9
3.57	3.60	3.58	3.67	3.74	3.83	3.88	3.99	3.81	3.87	3.99	4.07	3.95	4.03	3.80	3.85	3.95	3.97
16.4	17.5	16.5	16.4	16.2	16.6	16.1	15.8	16.2	14.3	13.6	13.8	13.5	13.9	15.1	15.1	15.6	15.0
7.45	7.64	7.47	7.42	7.37	7.31	6.97	6.82	6.10	9.26	8.77	8.93	7.37	7.44	6.35	6.23	6.23	6.14
1.63	1.67	1.65	1.61	1.59	1.60	1.55	1.50	1.34	1.85	1.78	1.79	1.59	1.58	1.27	1.28	1.23	1.33
60	50	<50	50	<50	70	50	50	60	140	70	80	90	70	70	70	50	80

(Continued)

GSR-3 Measured	GSR-3 Reported[a]	BCR-2 Measured	BCR-2 Reported[a]	BHVO-2 Measured	BHVO-2 Reported[a]

Major elements (wt%)

44.58	44.64
2.35	2.36
13.78	13.83
13.39	13.40
0.17	0.17
7.72	7.77
8.78	8.81
3.23	3.38
2.31	2.32
0.96	0.95
2.28	2.24
99.55	

Trace elements (ppm)

35.3	33	33.3	32
16.7	18	307	280
12.1	18	121	119
21.7	21	135	127
145	127	112	103
49.8	46.9	9.68	9.11
352	340	410	396
33.6	37	24.3	26
195	184	178	172
12.9	12.6	19.2	18.1
678	677	132	131
25.7	24.9	15.7	15.2
55.8	52.9	39.7	37.5
6.92	6.7	5.45	5.35
29.5	28.7	25.3	24.5
6.72	6.58	6.25	6.07
2.03	1.96	2.14	2.07
7.08	6.75	6.53	6.24
1.11	1.07	1	0.92
6.58	6.41	5.46	5.31

1.36	1.28	1.03	0.98
3.78	3.66	2.61	2.54
0.528	0.54	0.335	0.33
3.45	3.38	2.06	2
0.521	0.503	0.288	0.274
5.48	4.9	4.96	4.36
1.03	0.74	1.56	1.4
10.2	11	1.45	1.6
6.17	5.7	1.29	1.22
1.77	1.69	0.447	0.403
–		–	

Notes:

[a] Reported values for the reference materials are from GeoREM (http://georem.mpch-mainz.gwdg.de/).

[b] Total iron as Fe_2O_3; Mg# = $100 \times Mg^{2+}/(Mg^{2+} + Fe^{2+})$, assuming $Fe^{3+}/(Fe^{3+} + Fe^{2+}) = 0.28$.

Table S2 Rb–Sr, Sm–Nd isotopic compositions of the WEK basalts.

Sample	Data source	Rb (ppm)	Sr (ppm)	^{87}Rb/^{86}Sr	^{87}Sr/^{86}Sr	2σ	Sm (ppm)	Nd (ppm)	^{147}Sm/^{144}Nd	^{143}Nd/^{144}Nd	2σ	ε_{Nd}(0)[a]
SC1		104.1	1403	0.2148	0.705367	0.000007	10.85	66.12	0.0993	0.512391	0.000005	−4.8
SC2		105.4	1404	0.2172	0.705386	0.000007	10.81	65.85	0.0992	0.512408	0.000009	−4.5
GST1		87.67	1656	0.1532	0.705104	0.000014	9.78	58.44	0.1012	0.512404	0.000005	−4.6
GST2	This study	85.59	1579	0.1568	0.705085	0.000011	9.43	55.72	0.1024	0.512435	0.000004	−4.0
GST3		85.60	1572	0.1575	0.705028	0.000007	9.18	54.03	0.1027	0.512412	0.000005	−4.4
GST5		86.33	1589	0.1571	0.705057	0.000007	9.33	54.98	0.1026	0.512434	0.000005	−4.0
KL1		93.95	1590	0.1709	0.705203	0.000012	12.50	76.40	0.0990	0.512425	0.000010	−4.2
KL2		114.7	1516	0.2188	0.705459	0.000010	11.74	71.74	0.0989	0.512418	0.000007	−4.3
YQ1		103.9	1429	0.2104	0.705371	0.000012	11.09	68.03	0.0986	0.512408	0.000008	−4.5
YQ3		104.5	1445	0.2091	0.705412	0.000008	11.16	68.52	0.0985	0.512414	0.000005	−4.4
YQ4		103.8	1438	0.2089	0.705370	0.000008	11.15	68.44	0.0985	0.512429	0.000008	−4.1
YQ6		105.3	1447	0.2105	0.705383	0.000011	11.20	68.85	0.0984	0.512428	0.000005	−4.1
YQ7		105.6	1449	0.2108	0.705439	0.000012	11.20	68.80	0.0984	0.512423	0.000005	−4.2
YQ8		105.4	1448	0.2104	0.705420	0.000012	11.20	68.87	0.0984	0.512439	0.000004	−3.9
LHS1		105.8	1441	0.2124	0.705410	0.000008	11.13	68.50	0.0983	0.512407	0.000005	−4.5
LHS3		106.3	1438	0.2137	0.705414	0.000014	11.11	68.23	0.0985	0.512399	0.000006	−4.7
LHS4		111.7	1448	0.2231	0.705579	0.000008	11.00	68.06	0.0977	0.512400	0.000005	−4.6
LHS6	Chu et al. (2013)	87.73	1733	0.1464	0.705133	0.000010	13.66	82.66	0.0999	0.512464	0.000004	−3.4
LHS6		88.01	1733	0.1469	0.705151	0.000007	13.64	82.54	0.1000	0.512453	0.000005	−3.6
HSS2		93.86	1567	0.1732	0.705184	0.000008	12.06	72.08	0.1012	0.512474	0.000005	−3.2
HSS2		93.73	1564	0.1733	0.705133	0.000008	12.06	72.06	0.1012	0.512461	0.000006	−3.5
HSS5		91.90	1626	0.1634	0.705130	0.000008	12.46	74.45	0.1012	0.512453	0.000006	−3.6
HSS6		94.75	1330	0.2061	0.705273	0.000008	10.33	61.65	0.1013	0.512432	0.000004	−4.0
HSS8		95.17	1297	0.2123	0.705241	0.000012	10.38	61.68	0.1017	0.512418	0.000004	−4.3
KD1		106.1	1541	0.1992	0.705589	0.000008	10.84	67.91	0.0966	0.512362	0.000005	−5.4
KD3		102.9	1581	0.1883	0.705657	0.000011	10.21	63.58	0.0971	0.512342	0.000007	−5.8
KD4		105.1	1581	0.1923	0.705637	0.000010	10.18	63.35	0.0972	0.512344	0.000006	−5.7
KD5		103.5	1574	0.1901	0.705626	0.000007	10.36	64.58	0.0970	0.512347	0.000006	−5.7
BCR-2 Measured		46.9	340.2	0.398	0.705010	0.000011	6.563	28.68	0.1384	0.512664	0.000005	
BCR-2 Reported[b]		46.9	340		0.705000		6.58	28.7		0.512636		
BHVO-2 Measured		9.13	395.8	0.0667	0.703491	0.000007	6.081	24.52	0.1500	0.513002	0.000010	
BHVO-2 Reported[b]		9.11	396		0.703469		6.07	24.5		0.512980		

Notes:

[a] ε_{Nd}(0) values were calculated using (^{143}Nd/^{144}Nd)$_{CHUR}$(0) = 0.512638.

[b] Reported values for the reference materials are from GeoREM (http://georem.mpch-mainz.gwdg.de/).

Table S3 Clinopyroxene compositions of the WEK basalts.

Analyze Spot	Type[a]	SiO$_2$	TiO$_2$	Al$_2$O$_3$	Cr$_2$O$_3$	FeO[b]	NiO	MnO	MgO	CaO	Na$_2$O	K$_2$O	Mg#[c]	P (kbar)[d]	T (°C)[d]
YQ6-3.6	pc	49.62	2.25	3.48	0.16	6.87	0.00	0.13	14.63	21.90	0.61	0.04	79.1	2.0	1051
YQ6-3.7	pr	49.74	2.09	3.61	0.22	6.92	0.00	0.12	13.69	22.17	0.54	0.04	77.9	9.3	1104
YQ6-2.1	gm	50.46	1.81	2.69	0.17	7.13	0.00	0.09	14.66	21.61	0.47	0.03	78.6	4.5	1069
YQ6-2.2	pc	51.58	1.56	2.08	0.15	7.32	0.10	0.20	15.88	20.81	0.34	0.03	79.5	–	–
YQ6-2.3	pr	49.31	2.34	3.50	0.33	7.07	0.00	0.14	14.41	21.49	0.48	0.07	78.4	2.9	1059
YQ6-1.1	gm	48.97	2.41	3.81	0.28	6.82	0.09	0.15	13.57	22.86	0.45	0.04	78.0	4.2	1064
YQ6-1.2	gm	51.99	1.14	2.30	0.72	4.74	0.02	0.12	15.60	21.92	0.53	0.02	85.4	9.3	1104
HSS2-1.1	pc	52.36	0.96	1.77	0.46	4.88	0.07	0.07	15.88	22.83	0.46	0.04	85.3	6.2	1098
HSS2-1.2	pr	52.00	1.04	1.56	0.58	4.87	0.04	0.10	16.02	22.51	0.39	0.00	85.4	–	–
HSS2-1.3	pc	52.43	0.97	1.67	0.47	4.89	0.02	0.14	15.88	22.53	0.38	0.00	85.3	7.5	1108
HSS2-1.4	pr	51.03	1.48	2.84	0.93	5.13	0.00	0.11	15.18	22.75	0.51	0.05	84.1	6.6	1103
HSS2-1.5	pc	52.37	1.06	1.88	0.23	5.23	0.02	0.17	15.78	22.35	0.48	0.01	84.3	9.1	1121
HSS2-1.6	pr	49.94	1.82	3.35	0.43	6.07	0.08	0.13	14.33	22.56	0.45	0.01	80.8	9.5	1125
HSS2-1.7	pc	52.67	1.00	1.62	0.56	4.71	0.09	0.12	16.02	22.57	0.46	0.01	85.8	6.5	1101
HSS2-1.8	pr	50.86	1.15	2.55	0.87	5.04	0.01	0.07	15.28	22.81	0.64	0.01	84.4	4.2	1084
HSS2-1.9	pc	50.53	1.41	3.10	0.33	5.78	0.04	0.10	14.92	22.36	0.47	0.00	82.1	10.9	1136
HSS2-1.10	pr	51.18	1.49	2.77	0.57	5.35	0.09	0.10	15.04	22.51	0.46	0.02	83.4	10.0	1129
HSS2-2.1	pc	52.89	1.03	1.75	0.34	5.29	0.00	0.08	15.99	22.50	0.41	0.01	84.3	8.4	1116
HSS2-2.2	pr	51.61	1.47	2.73	0.76	5.29	0.05	0.06	15.04	23.19	0.42	0.02	83.5	8.3	1115
HSS2-2.3	pc	52.10	1.13	2.08	0.28	5.53	0.02	0.11	16.05	21.78	0.38	0.01	83.8	9.3	1124
HSS2-2.4	pr	49.92	2.00	3.57	0.25	6.15	0.04	0.13	14.67	22.62	0.46	0.03	81.0	8.2	1115
HSS2-2.5	pc	49.30	2.41	3.99	0.28	6.43	0.00	0.13	14.09	22.89	0.43	0.00	79.6	7.5	1110
HSS2-2.6	pr	49.67	2.20	3.62	0.63	6.19	0.02	0.09	14.28	22.35	0.52	0.03	80.4	7.8	1114
HSS2-3.1	pc	52.30	0.96	1.62	0.43	4.96	0.05	0.07	16.00	22.41	0.44	0.00	85.2	6.0	1097
HSS2-3.2	pr	50.97	1.99	3.40	0.61	5.77	0.02	0.08	14.61	22.02	0.53	0.05	81.9	12.2	1149
HSS2-3.3	pc	51.39	1.46	2.32	0.12	6.19	0.00	0.13	15.28	22.02	0.40	0.02	81.5	8.1	1115
HSS2-3.4	pr	46.70	2.90	5.88	0.07	8.27	0.02	0.13	12.81	22.57	0.60	0.06	73.4	–	–
HSS2-3.5	pc	52.05	1.15	1.78	0.16	5.76	0.02	0.15	16.08	21.97	0.40	0.00	83.3	3.7	1081
HSS2-3.6	pr	51.67	1.52	3.01	0.71	5.26	0.09	0.11	15.41	21.83	0.51	0.02	83.9	12.3	1149
HSS5-3.1	pc	52.94	1.08	2.14	0.13	5.57	0.08	0.14	15.25	22.82	0.39	0.01	83.0	11.6	1140
HSS5-3.2	pr	51.71	1.52	3.13	0.64	5.54	0.02	0.13	15.56	21.61	0.47	0.01	83.4	12.7	1154
HSS5-3.3	pc	52.51	1.15	1.92	0.12	5.69	0.01	0.12	15.84	22.16	0.37	0.00	83.2	9.5	1125
HSS5-3.4	pr	50.18	1.99	3.88	0.71	5.96	0.07	0.12	14.67	22.48	0.48	0.03	81.4	10.3	1134
HSS5-3.5	pc	49.91	2.20	4.11	0.52	6.34	0.01	0.11	14.43	22.33	0.51	0.02	80.2	11.0	1140
HSS5-3.6	pr	48.80	2.50	3.38	0.04	7.63	0.00	0.11	13.60	22.86	0.60	0.05	76.1	–	–
HSS5-3.7	pc	50.87	1.83	3.64	0.19	6.50	0.07	0.13	15.29	20.94	0.54	0.02	80.7	13.5	1162
HSS5-3.8	pr	53.00	0.97	1.68	0.39	5.13	0.05	0.08	16.39	22.56	0.32	0.00	85.1	6.3	1101
HSS5-2.1	pc	52.68	1.23	1.96	0.02	5.93	0.05	0.13	15.84	22.27	0.47	0.00	82.6	8.8	1120

HSS5-2.2	pr	51.97	1.66	3.05	0.74	5.54	0.00	0.16	15.03	21.74	0.48	0.01	82.9	12.9	1155
HSS5-2.3	pc	53.03	1.03	1.65	0.27	5.46	0.11	0.15	16.50	21.76	0.36	0.01	84.3	8.2	1117
HSS5-2.4	pr	48.02	3.34	3.82	0.07	7.87	0.01	0.13	13.07	22.22	0.69	0.03	74.8	–	–
HSS5-2.5	pc	53.01	1.13	1.92	0.02	5.75	0.08	0.13	16.01	21.87	0.37	0.00	83.2	11.3	1140
HSS5-2.6	pr	53.85	0.89	1.53	0.51	4.75	0.00	0.15	16.41	21.76	0.36	0.00	86.0	11.3	1140
HSS5-2.7	pc	53.23	1.04	1.74	0.30	5.34	0.05	0.16	16.28	21.77	0.41	0.00	84.5	10.5	1135
HSS5-2.8	pr	51.25	1.99	2.95	0.46	6.05	0.00	0.12	14.73	21.65	0.51	0.04	81.3	11.4	1143
HSS5-1.1	pc	52.16	1.07	2.10	0.06	5.50	0.00	0.12	15.25	22.76	0.46	0.00	83.2	10.8	1133
HSS5-1.2	pr	50.76	1.78	3.40	0.39	5.94	0.07	0.07	14.52	22.37	0.45	0.00	81.3	12.4	1149
HSS5-1.3	pc	49.74	1.92	3.48	0.00	6.86	0.06	0.11	13.92	22.47	0.51	0.00	78.3	10.8	1135
HSS5-1.4	pr	50.99	1.48	2.69	0.08	6.24	0.06	0.12	14.92	22.15	0.48	0.00	81.0	10.2	1131
HSS5-1.5	pc	50.68	1.66	3.00	0.37	5.72	0.11	0.12	14.74	22.26	0.41	0.01	82.1	11.0	1137
HSS5-1.6	pr	50.85	1.83	2.74	0.48	5.82	0.00	0.03	14.59	22.36	0.41	0.02	81.7	9.2	1124
HSS5-1.7	pc	50.74	1.71	2.32	0.06	6.97	0.01	0.15	14.28	22.66	0.64	0.00	78.5	–	–
HSS5-1.8	pr	50.92	1.73	2.43	0.28	6.36	0.00	0.10	13.83	23.07	0.44	0.03	79.5	8.1	1111
YQ8-3.1	gm	51.31	1.40	1.79	0.26	6.52	0.00	0.22	15.75	21.67	0.44	0.05	81.2	–	–
YQ8-3.2	gm	50.85	1.87	2.58	0.06	7.49	0.06	0.12	14.75	21.62	0.42	0.09	77.8	–	–
YQ8-3.3	gm	50.48	2.02	3.26	0.39	7.30	0.07	0.11	14.08	21.47	0.56	0.12	77.5	–	–
YQ8-3.4	gm	49.07	2.63	3.93	0.60	7.01	0.00	0.06	13.90	22.23	0.59	0.09	77.9	–	–
YQ8-3.5	gm	50.98	1.99	2.94	0.15	7.38	0.03	0.13	14.56	21.17	0.53	0.05	77.9	–	–
YQ8-1.1	gm	51.57	1.49	2.07	0.29	6.31	0.02	0.14	15.86	21.90	0.49	0.07	81.8	–	–
YQ8-1.2	gm	51.54	1.48	2.07	0.50	5.94	0.01	0.14	15.44	21.42	0.70	0.15	82.2	4.4	1131
YQ8-1.3	gm	49.34	2.14	3.54	0.36	7.15	0.02	0.13	14.42	21.73	0.47	0.05	78.2	4.8	1136
YQ8-1.4	gm	49.18	2.39	3.63	0.20	7.69	0.04	0.19	13.83	21.35	0.56	0.08	76.2	–	–
YQ8-1.5	gm	49.48	2.16	3.34	0.16	7.37	0.03	0.14	14.21	21.65	0.44	0.05	77.5	–	–
YQ8-1.6	gm	51.94	1.26	1.86	0.71	5.52	0.03	0.13	16.23	21.58	0.41	0.07	84.0	–	–
YQ8-1.7	gm	49.78	2.37	3.67	0.22	7.34	0.02	0.15	13.41	21.80	0.60	0.22	76.5	–	–
KD1-1.1	gm	50.22	3.05	4.60	0.03	8.29	0.06	0.10	13.20	21.69	0.58	0.08	73.9	–	–
KD1-1.2	gm	51.18	2.25	3.02	0.30	7.07	0.00	0.07	14.62	21.73	0.40	0.02	78.7	10.3	1146
KD1-1.3	gm	47.60	3.42	5.47	0.03	9.37	0.00	0.16	12.50	21.18	0.63	0.02	70.4	–	–
KD1-1.4	gm	50.11	1.90	2.63	0.25	7.43	0.08	0.15	15.09	21.16	0.43	0.03	78.4	–	–
KD1-1.5	gm	52.46	1.43	1.85	0.34	6.28	0.01	0.14	15.70	21.68	0.34	0.03	81.7	7.8	1125
SC2-1.1	gm	49.83	1.94	3.46	0.22	6.52	0.00	0.09	14.72	22.33	0.64	0.03	80.1	6.2	1101
SC2-1.2	gm	50.93	1.28	2.90	1.03	5.49	0.07	0.13	15.60	22.15	0.60	0.05	83.5	5.3	1095
SC2-1.3	gm	50.99	1.57	2.06	0.07	6.97	0.01	0.18	15.22	22.51	0.45	0.03	79.6	–	–
SC2-1.4	gm	49.90	2.12	3.08	0.07	7.55	0.04	0.14	14.70	21.55	0.35	0.07	77.6	1.3	1065
SC2-2.3	gm	48.56	2.49	3.95	0.12	7.64	0.06	0.09	13.79	21.79	0.53	0.09	76.3	–	–
SC2-2.4	gm	49.56	2.49	3.79	0.33	7.04	0.04	0.16	14.01	21.41	0.53	0.06	78.0	10.6	1137
SC2-2.5	gm	49.51	2.47	3.56	0.12	7.49	0.06	0.10	13.82	22.86	0.57	0.12	76.7	–	–
HSS5-CPXP-3-CORE	pc	50.55	1.7	2.25	0.23	6.30	0.02	0.12	15.55	22.37	0.37	0.04	81.5	–	–
HSS5-CPXP-3-RIM	pr	44.6	2.76	4.60	0.00	7.40	0.00	0.07	11.97	23.76	0.56	0.03	74.2	–	–

HSS5-CPXP-1-1	pr	47.4	2.67	4.78	0.22	6.48	0.09	0.07	13.43	22.35	0.50	0.05	78.7	10.2	1133
HSS5-CPXP-1-2	pr	51.54	1.2	1.89	0.19	5.32	0.04	0.13	15.96	22.33	0.27	0.02	84.2	2.0	1067
HSS5-CPXP-1-3	pc	51.78	0.99	1.74	0.25	5.48	0.00	0.10	15.82	22.54	0.30	0.00	83.7	3.0	1074
HSS5-CPXP-1-4	pr	48.66	1.97	4.06	0.37	6.23	0.00	0.14	14.37	22.41	0.49	0.00	80.4	8.7	1121
HSS5-CPXP-1-5	pr	51.63	0.95	1.77	0.44	4.63	0.00	0.06	15.72	23.36	0.39	0.04	85.8	–	–
HSS5-CPXP-2-1	pr	49.59	1.96	3.49	0.58	5.63	0.03	0.06	14.83	22.89	0.51	0.01	82.4	0.8	1060
HSS5-CPXP-2-2	pc	48.91	1.91	3.65	0.05	6.58	0.04	0.21	14.20	22.77	0.43	0.00	79.4	6.5	1102
HSS5-CPXP-2-3	pc	51.22	1.23	1.93	0.00	6.03	0.02	0.16	15.40	22.63	0.37	0.00	82.0	–	–
HSS5-CPXP-2-4	pc	51.53	1.00	1.69	0.13	5.39	0.01	0.11	15.94	22.28	0.29	0.00	84.1	2.6	1071
HSS5-CPXP-2-5	pr	50.24	1.59	2.92	0.67	5.16	0.02	0.20	14.69	23.09	0.45	0.02	83.5	5.5	1094
HSS5-CPXP-4-1	pr	49.78	1.68	3.08	0.40	5.65	0.04	0.19	14.91	22.69	0.42	0.00	82.5	3.3	1078
HSS5-CPXP-4-2	pc	47.43	2.51	4.40	0.08	7.23	0.05	0.06	13.52	22.45	0.48	0.00	76.9	5.1	1093
HSS5-CPXP-4-3	pc	52.06	1.28	1.87	0.13	5.89	0.00	0.18	15.77	22.38	0.31	0.00	82.7	3.5	1079
HSS5-CPXP-4-4	pc	51.27	1.22	1.83	0.16	5.69	0.00	0.11	15.66	22.55	0.31	0.00	83.1	–	–
HSS5-CPXP-4-5	pr	47.81	2.17	4.09	0.00	7.54	0.02	0.17	13.22	22.99	0.52	0.01	75.8	–	–
YQ6-CPXM-1	gm	49.32	1.94	2.99	0.41	7.10	0.06	0.10	14.71	21.42	0.42	0.06	78.7	–	–
HSS2-CPXP-1-C	pc	51.7	1.26	2.00	0.16	5.91	0.00	0.14	16.06	21.31	0.29	0.02	82.9	7.8	1114
HSS2-CPXP-1-R	pr	47.37	2.59	4.66	0.23	6.71	0.00	0.09	13.72	22.64	0.47	0.03	78.5	5.1	1093
HSS2-CPXP-2-C	pc	49.42	1.61	2.77	0.48	6.04	0.03	0.12	14.89	22.49	0.45	0.01	81.5	–	–
HSS2-CPXP-2-R	pr	47.89	2.71	4.77	0.06	7.82	0.00	0.15	13.09	22.09	0.57	0.04	74.9	–	–
HSS2-CPXP-3-C	pc	50.98	1.42	2.26	0.03	6.01	0.04	0.14	15.27	22.50	0.40	0.00	81.9	3.3	1076
HSS2-CPXP-3-R	pr	49.43	1.81	3.55	0.41	6.20	0.06	0.17	14.30	22.28	0.49	0.07	80.4	9.6	1127
HSS2-CPXP-4-C	pc	52.86	0.8	2.17	0.49	4.48	0.00	0.13	16.68	21.72	0.58	0.00	86.9	11.9	1146
HSS2-CPXP-4-R	pr	50.31	1.38	2.81	0.60	5.39	0.00	0.11	15.09	22.85	0.49	0.00	83.3	3.7	1080
HSS2-CPXP-5-C	pc	52.41	0.99	1.59	0.23	4.81	0.07	0.11	15.74	23.12	0.33	0.01	85.4	6.3	1097
HSS2-CPXP-5-R	pr	50.57	1.38	2.91	0.89	5.13	0.02	0.10	15.20	22.77	0.45	0.00	84.1	6.0	1099
HSS2-CPXP-6-C	pc	50.02	1.7	3.13	0.67	5.73	0.06	0.09	15.02	22.57	0.49	0.00	82.4	1.8	1067
HSS2-CPXP-6-R	pr	45.93	2.62	4.91	0.02	8.72	0.00	0.16	11.84	22.82	0.68	0.04	70.8	–	–
HSS2-CPXM-1	gm	48.66	2.33	3.95	0.00	8.04	0.04	0.16	13.77	22.28	0.54	0.09	75.3	–	–
HSS2-CPXM-2	gm	50.16	1.84	2.72	0.03	7.20	0.03	0.17	14.38	22.20	0.44	0.07	78.1	2.1	1069
HSS2-CPXM-3	gm	50.62	1.62	2.57	0.00	7.23	0.05	0.21	14.36	21.98	0.38	0.06	78.0	8.3	1116
HSS2-CPXM-4	gm	47.32	2.67	4.44	0.08	8.02	0.00	0.15	12.86	22.54	0.52	0.06	74.1	–	–
HSS2-CPXM-5	gm	47.22	2.09	3.64	0.49	7.32	0.06	0.11	16.19	21.21	0.45	0.04	79.8	–	–
HSS2-CPXM-6	gm	50.39	1.64	2.36	0.00	6.91	0.00	0.13	14.61	22.67	0.45	0.00	79.0	–	–
YQ8-CPXM-1	gm	47.35	2.73	4.52	0.12	8.24	0.11	0.20	13.41	21.24	0.57	0.07	74.4	–	–
YQ8-CPXM-2	gm	47.82	2.67	4.08	0.34	6.93	0.00	0.08	13.72	22.46	0.53	0.07	77.9	–	–
YQ8-CPXM-3	gm	51.11	1.47	1.89	0.17	7.28	0.05	0.17	15.74	21.18	0.37	0.05	79.4	–	–
YQ8-CPXM-4	gm	50.02	1.63	2.31	0.02	6.45	0.11	0.20	14.35	22.31	0.44	0.08	79.9	1.2	1103
YQ8-CPXM-5	gm	50.56	1.92	4.15	0.01	6.80	0.00	0.12	13.74	19.59	0.56	0.79	78.3	–	–
YQ8-CPXP-1-C	pc	50.48	1.65	2.38	0.03	6.83	0.00	0.18	14.91	22.25	0.42	0.04	79.6	–	–
YQ8-CPXP-1-R	pr	50.83	1.63	2.18	0.02	7.15	0.00	0.15	15.13	21.85	0.47	0.05	79.0	–	–

YQ8-CPXM-6	gm	49.91	1.64	2.51	0.25	7.20	0.06	0.20	15.39	21.10	0.32	0.06	79.2	–	–
YQ8-CPXM-7	gm	50.89	1.73	2.19	0.01	7.19	0.05	0.12	14.88	22.08	0.43	0.05	78.7	–	–

Notes:

[a] "pr" denotes phenocryst rim; "pc" denotes phenocryst core; "gm" denotes groundmass clinopyroxene.

[b] Total iron as FeO.

[c] Mg# = $100 \times Mg/(Mg+Fe^{2+})$, where Mg and Fe^{2+} are cation molar fractions. Fe^{2+} proportion is set to be 100%.

[d] Temperatures and pressures are calculated using the thermobarometer of Putirka et al. (2003); "–" represents no valid P–T result.

Figure S1
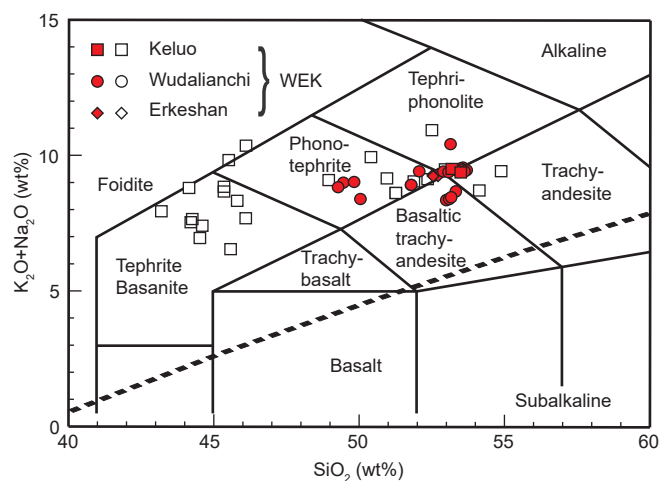
Figure S1. Total alkali vs. SiO₂ content (TAS) diagram for the Wudalianchi, Erkeshan, and Keluo potassic volcanic rocks. Rock classification is after Le Bas et al. (1986). Data sources: Zhang (1992), Zhang et al. (1995), Chu et al. (2013), and this study. Our 26 samples are marked in red.
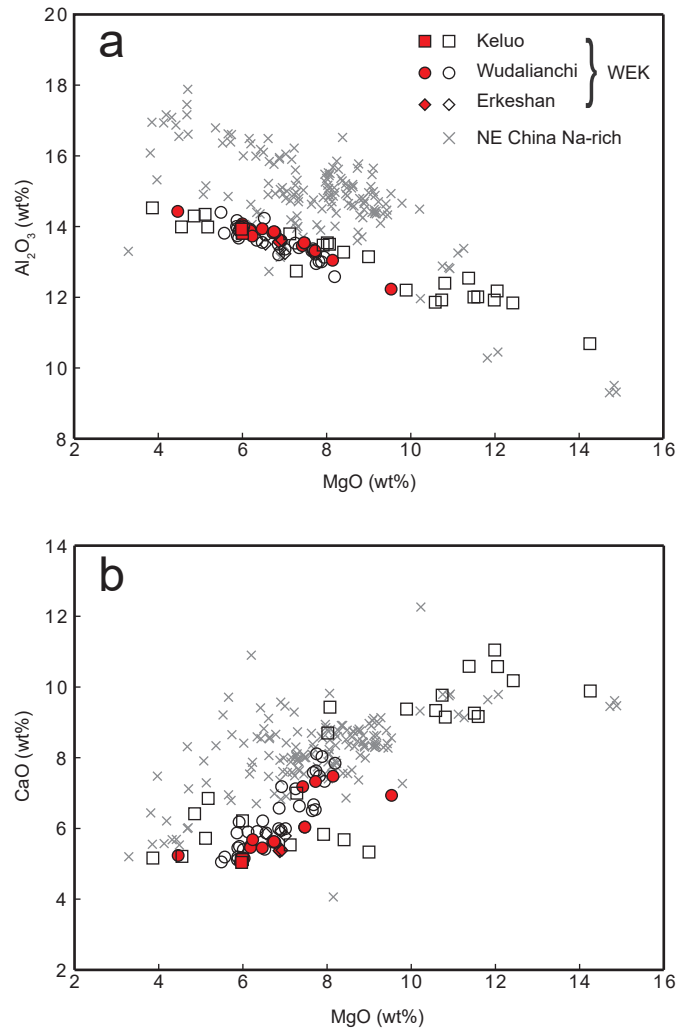
Figure S2

Figure S2. Whole-rock (a) CaO vs. MgO and (b) Al₂O₃ vs. MgO content diagrams for the Wudalianchi, Erkeshan, and Keluo potassic basalts, and other Cenozoic Na-rich basalts from NE China. Data sources: Zhang (1992), Zhang et al. (1995), Basu et al. (1991), Liu et al. (1994), Zou et al. (2003), Chen et al. (2007), Yan and Zhao (2008), and Chu et al. (2013) and this study. Our 26 samples are marked in red.
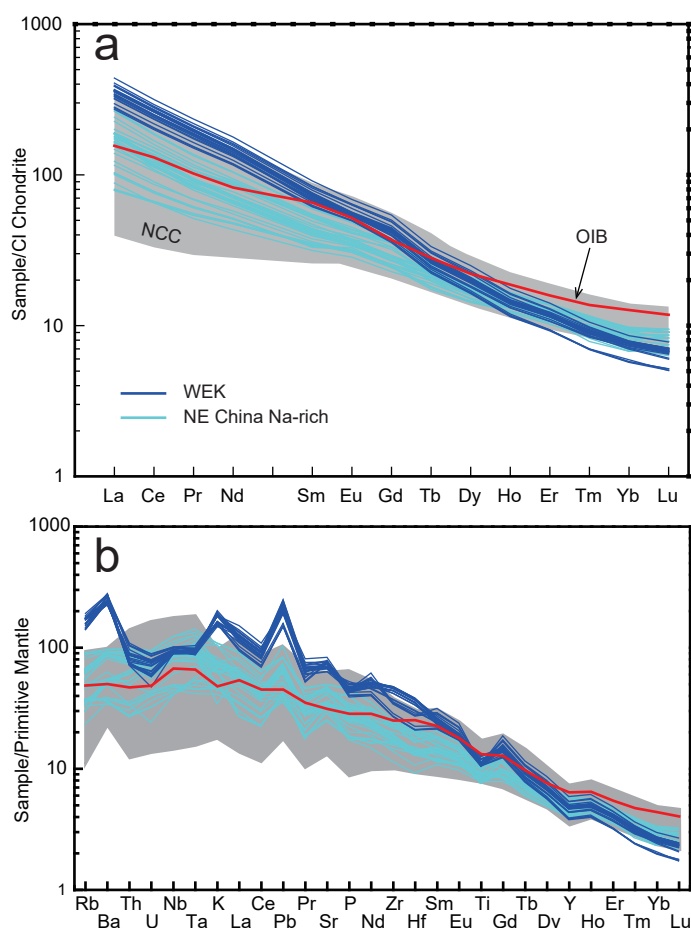
Figure S3

Figure S3. (a) CI Chondrite-normalized rare earth element diagram and (b) primitive-mantle-normalized trace element diagram for the WEK potassic basalts and other Na-rich Cenozoic basalts from NE China. The field of Cenozoic Na-rich basalts from the North China Craton (NCC) is also shown. Data sources: CI chondrite, primitive mantle, and OIB from Sun and McDonough (1989); NE China from Chen et al. (2015); WEK from Chu et al. (2013) and this study; NCC from Xu et al. (2005, 2012), Tang et al. (2006), and Sakuyama et al. (2013). The elements in (b) are in order of increased incompatibility, after Sun and McDonough (1989).
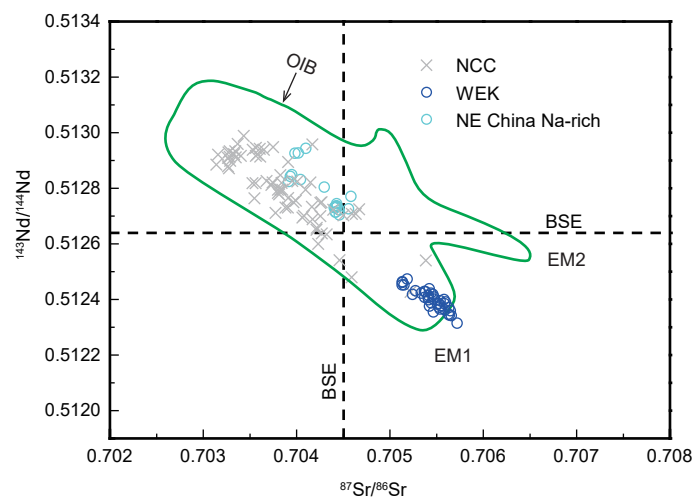
Figure S4

Figure S4. Sr–Nd isotope diagram for the WEK potassic basalt and other Cenozoic Na-rich basalts from NE China and the North China Craton (NCC). OIB, BSE, EM1, and EM2 data are from Zindler and Hart (1986). Data sources for NE China and the NCC are the same as Fig. S3. Data for WEK are from Chu et al. (2013), Sun et al. (2014), and the present study.
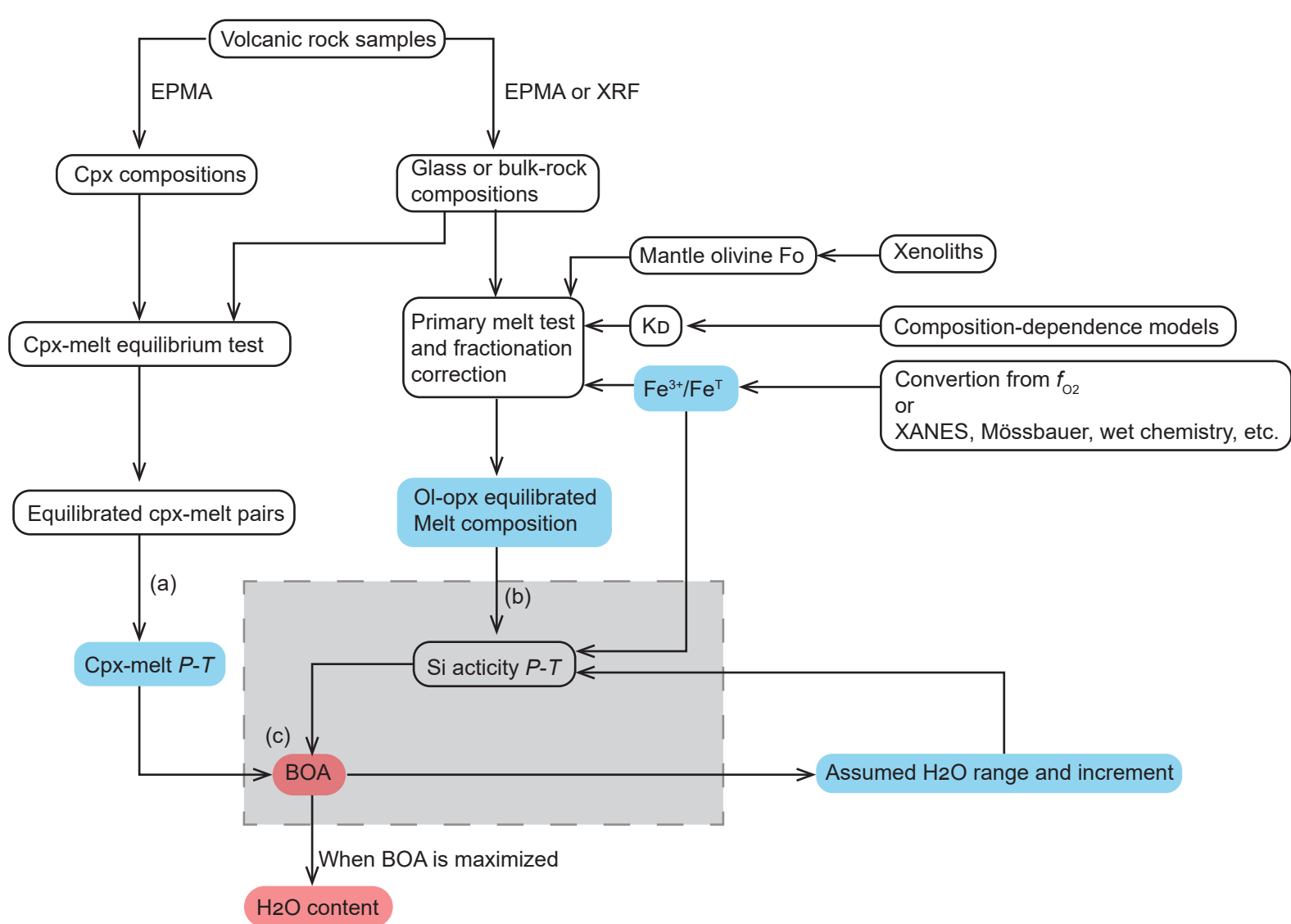
Figure S5. Flow chart of the water content estimation method used in this study. The calculation steps in the gray field (i.e., b and c) correspond to the Python program provided in Appendix C. Elements in blue are the required input for the program; elements in red are the output of the program. BOA, buffer overlapping area.